-Electronic Supplementary Information (ESI)-

Sulakshana Shenoy,[a] Chitiphon Chuaicham,[a] Keiko Sasaki,[a]* Sungkyun Park,[b] Muthuchamy Nallal,[b,c]* Kang Hyun Park,[c]* and Karthikeyan Sekar[d]*

[a] *Department of Earth Resources Engineering, Kyushu University, Fukuoka 819-0395, Japan. Email: keikos@mine.kyushu-u.ac.jp*
[b] *Department of Physics, Pusan National University, Busan46241, Republic of Korea. Email: muthuchamyn89@gmail.com*
[c] *Department of Chemistry, Pusan National University, Busan 46241, Republic of Korea. Email: chemistry@pusan.ac.kr*
[d] *Department of Chemistry, SRM Institute of Science and Technology, Kattankulathur 603203, Chennai, Tamil Nadu, India. Email: karthiks13@srmist.edu.in*

Experimental Section

All the raw materials utilized in the experiment were of analytical grade and used without undergoing additional purification. The precise quantities of each precursor utilized in the synthesis are outlined in Table S1. Typically, 5.62 g of $CoSO_4.7H_2O$, 1.8 g of $(NH_4)_2S_2O_8$ and 0.5 g of melamine were dissolved in 40 ml of deionized water (DI H_2O). 2.47 g of $(NH_4)_6Mo_7O_{24}.4H_2O$ was further added to the above solution and stirred continuously for 10 min. The reaction mixture was transferred to a Teflon-lined stainless autoclave and treated at 180 ^oC, 24 h. The obtained precipitates were washed repeatedly with DI H_2O and ethanol, dried at 60 ^oC for 12 h. The sample obtained after drying were calcined at 400 ^oC for 4 h. The synthesis procedure for obtaining tube-like structures of Co-Mo is analogous, with the exception that the structure directing agent is substituted with urea. In order to establish a basis for comparison, Co-Mo structures were synthesized in the absence of urea and melamine.

Table S1 presents the specific quantities of the various precursors used during the synthesis of Co-Mo heterostructures.

Cobalt (II) sulfate heptahydrate ($CoSO_4.7H_2O$)	Ammonium molybdate tetrahydrate $(NH_4)_6Mo_7O_{24}.4H_2O$)	Ammonium peroxodisulfate $(NH_4)_2S_2O_8$)	Melamine ($C_3H_6N_6$)	Urea (CH_4N_2O)	Sample label
0.02 M, 5.62 g	0.002 M, 2.47 g	1.8 g	0.5 g	-	Co-Mo HNS
0.02 M, 5.62 g	0.002 M, 2.47 g	1.8 g	-	0.5 g	Co-Mo HNT
0.02 M, 5.62 g	0.002 M, 2.47 g	1.8 g	-	-	Co-Mo Control

Characterization

The X-ray diffraction patterns of the as-synthesized electrocatalysts were observed on Rigaku Ultima IV diffractometer. Keyence VE-9800 scanning electron microscope and Hitachi JEM-ARM200F transmission electron microscope were used to analyse the morphology and microstructure of the synthesized samples. Surface compositions and chemical bonding states were analysed by X-ray photoelectron spectroscopy, ESCA 5800, ULVAC-PHI X. The orbitals were calibrated by the binding energies of [C 1s] at E = 284.6 eV. Transmission mode Co *K*-edge X-ray Absorption Near Edge Spectroscopy (XANES) at SAGA Light Source (SAGA-LS) located at the BL06 Research Centre for Synchrotron Light Application at Kyushu University was used to measure the as-synthesized catalysts and Co standards. After diluting the samples with boron nitride, they were secured with Kapton tape. We were able to scan the photon energy from 8.9 to 9.2 keV by using a silicon double crystal monochromator. 1.40 GeV resulted in a storage ring current of 306.1 mA. A linear combination fitting study was conducted using the Athena-Demeter 0.9.26 tool from the IFEFFIT software suite. For the fitting parameter for EXAFS analysis, the result was considering at k-range between 3-9 $Å^{-1}$ and r-range between 1-3.3 Å with Hanning window and fitting k weights=3. The model for the EXAFS was produced *via* a path-like function of cobalt oxide to generate a single scattering path of arbitrary length.

Electrochemical measurements

The electrochemical measurements of the synthesized electrocatalysts were conducted on a standard electrochemical workstation (CHI600E CH Instruments; Pine Research Instruments) and a three-electrode system in an alkaline medium (1.0 M KOH). For the counter and reference electrodes, we utilized a commercially available graphite rod (d=6 mm) and a saturated calomel electrode (SCE) respectively. The glassy carbon electrode (GCE) loaded with an electrocatalyst was chosen as the working electrode, with a surface area of 0.1963 cm^2. As a first step, an electrocatalyst slurry was made by ultrasonically mixing 2 mg of catalyst with 0.49 mL of 2-propanol, 0.49 mL of ultrapure DI water, and 0.02 mL of 5% Nafion. The homogenized slurry was drop-casted onto pre-treated GCE and dried at room temperature (catalyst quantity, 0.0815 mg cm^{-2}). The measured potentials were normalized using the reversible hydrogen electrode (RHE) potential as the standard potential with the following equation: E(RHE) = E(SCE) + 0.241 + 0.059 pH. The scan rate of the linear sweep voltammetry (LSV) was 5 mV s^{-1}. The OER and HER performance of the electrocatalysts were assessed

using cyclic voltammetry (CV) and chronoamperometry (CA) measurements using iR corrected values. The Tafel equation ($\eta = b \log j + a$, where j is the current density and b is the Tafel slope) is used to fit the linear part of the Tafel plots.

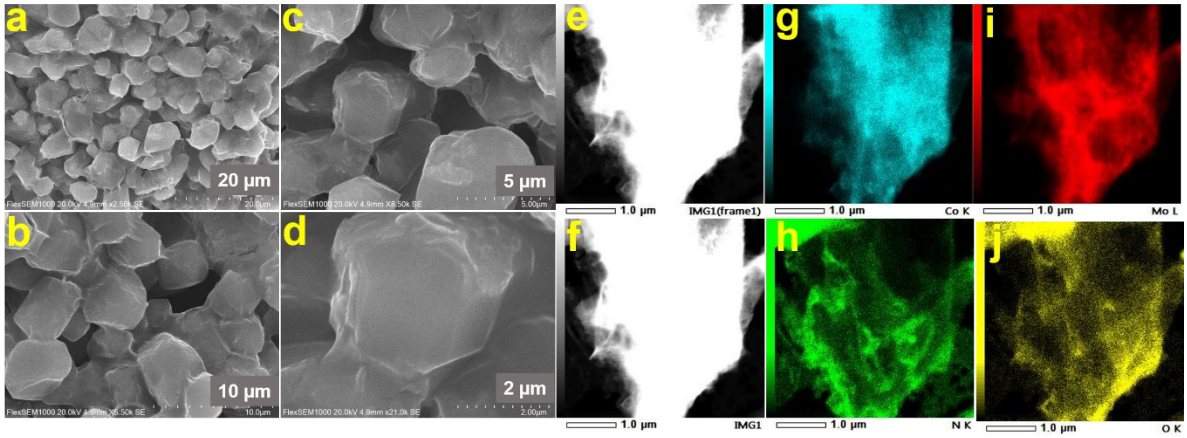

Fig. S1 (a-d) Low-magnification SEM images, (e,f) TEM images and (g-j) TEM-EDX mapping of Co, Mo, N and O in Co-Mo control.

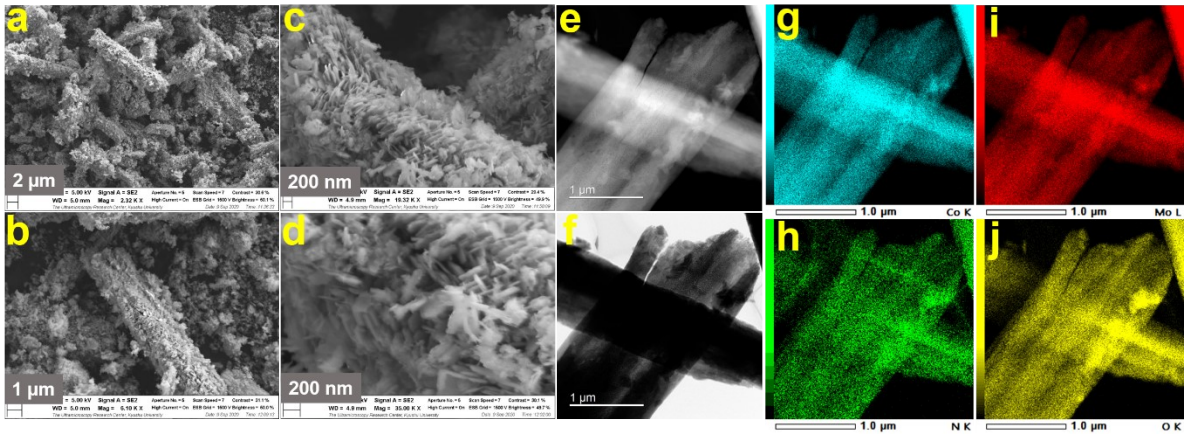

Fig. S2 (a-d) Low-magnification SEM images, (e,f) TEM images and (g-j) TEM-EDX mapping of Co, Mo, N and O in Co-Mo HNT.

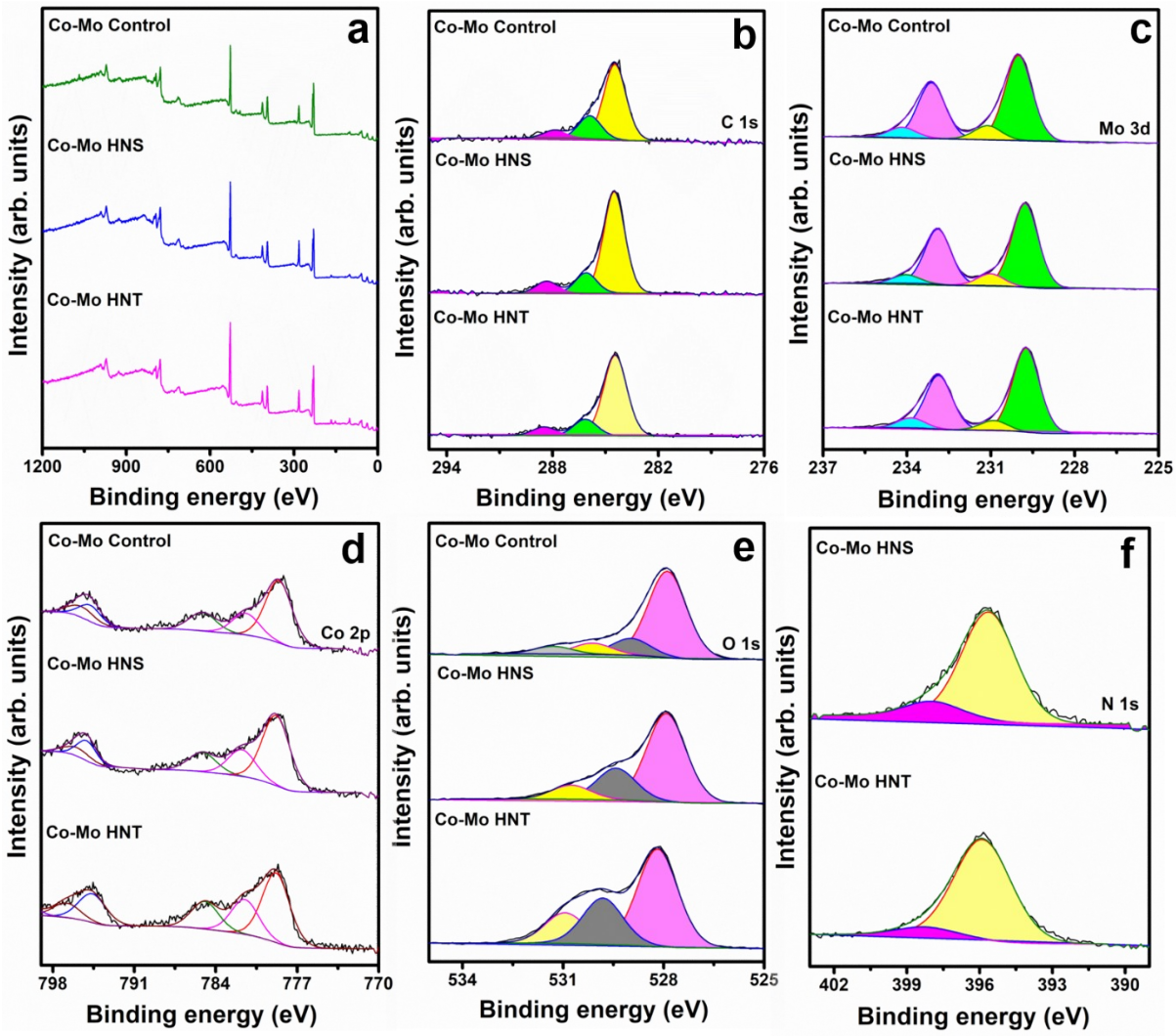

Fig. S3 (a) XPS survey spectra, deconvoluted spectra (b) C 1s, (c) Mo 3d, (d) Co 2p, (e) O1s and (f) N 1s in Co-Mo heterostructures.

Table S2 EXAFS fitting parameters for Co-Mo Control, HNS and HNT.

Co *K*-edge				
Samples	**Atom type**	**Coordination number**	**Distance R (Å)**	**Debye-Waller factor σ^2 (10^{-3}. Å^2)**
Co-Mo Control	Co-O	2.020	1.95	3.55
	Co-Mo	1.542	2.73	3.55
	Co-Co	2.020	3.29	3.55
Co-Mo HNS	Co-O	4.072	2.02	6.97
	Co-Mo	4.072	2.97	6.97
	Co-Co	4.072	3.64	6.97
Co-Mo HNT	Co-O	4.156	1.85	3.00
	Co-Mo	4.156	2.71	2.72
	Co-Co	3.732	3.27	3.00

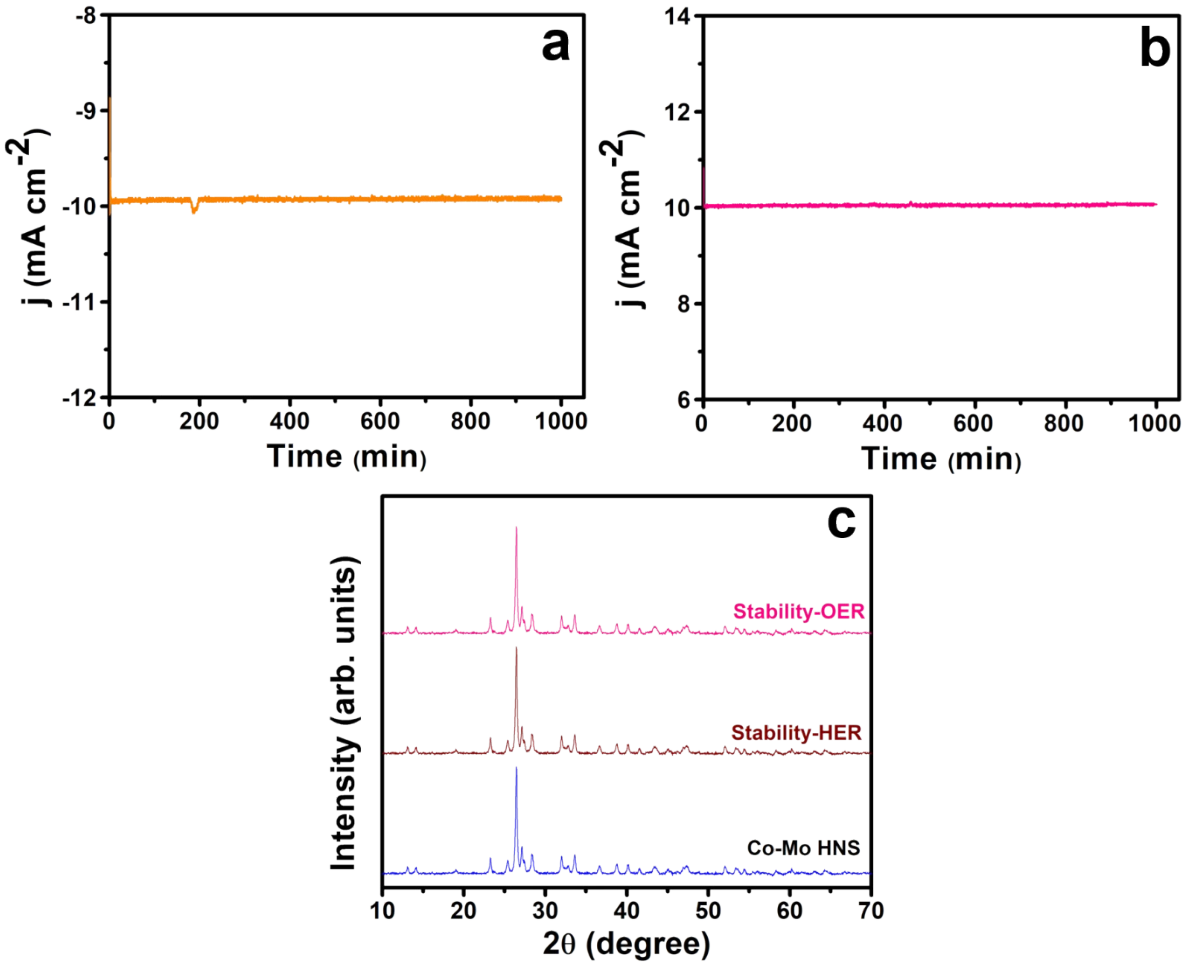

Fig. S4 (a) Current density curve observed over 17 h, while maintaining a static potential of (a) -0.280 V in HER, (b) +1.519 V in OER and (c) XRD patterns of Co-Mo HNS after HER and OER tests.

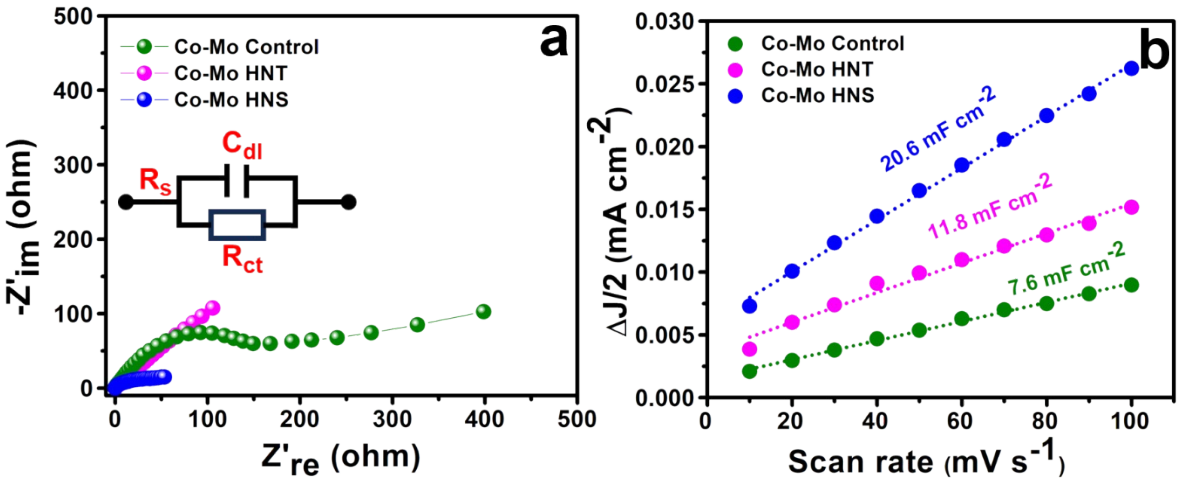

Fig. S5 (a) Nyquist plots of Co-Mo electrocatalysts with fitting curves, inset Randle's circuit and (b) scan rate vs. capacitive current plots with linear slopes.

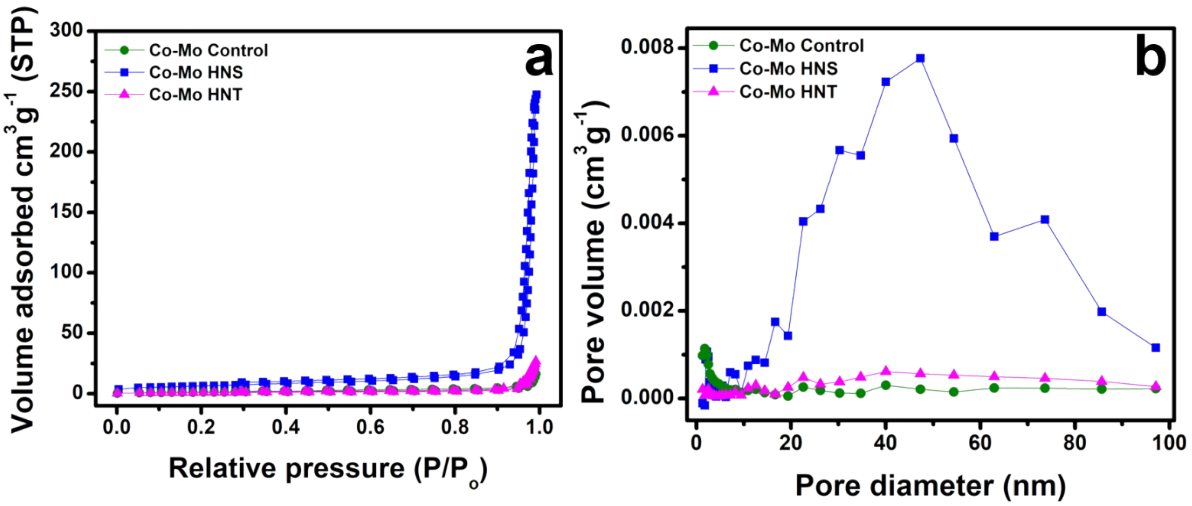

Fig. S6 (a) Isotherm for nitrogen adsorption–desorption and (b) distribution of pore size in Co-Mo Control, HNS and HNT respectively.

Table S3 represents the values for ESCA, BET surface area, pore volume, roughness factor and R_{ct} for Co-Mo heterostructures.

Sample	**ESCA (cm^2)**	**BET surface area (m^2g^{-1})**	**Pore volume (cm^3g^{-1})**	**Roughness factor**	**R_{ct} (ohms)**
Co-Mo Control	7.75	5	0.02	39.5	175
Co-Mo HNS	21.6	23	0.36	107	18
Co-Mo HNT	12.04	9	0.04	61.33	32

The electrochemical active surface area (ECSA) = $\frac{C_{dl}\, value\ of\ catalyst}{C_{dl}\, value\ of\ GC\ matrix}$

Roughness factor (RF) = $\frac{ECSA}{A}$

Where, A is the area of the GC electrode (0.1963 cm^2)

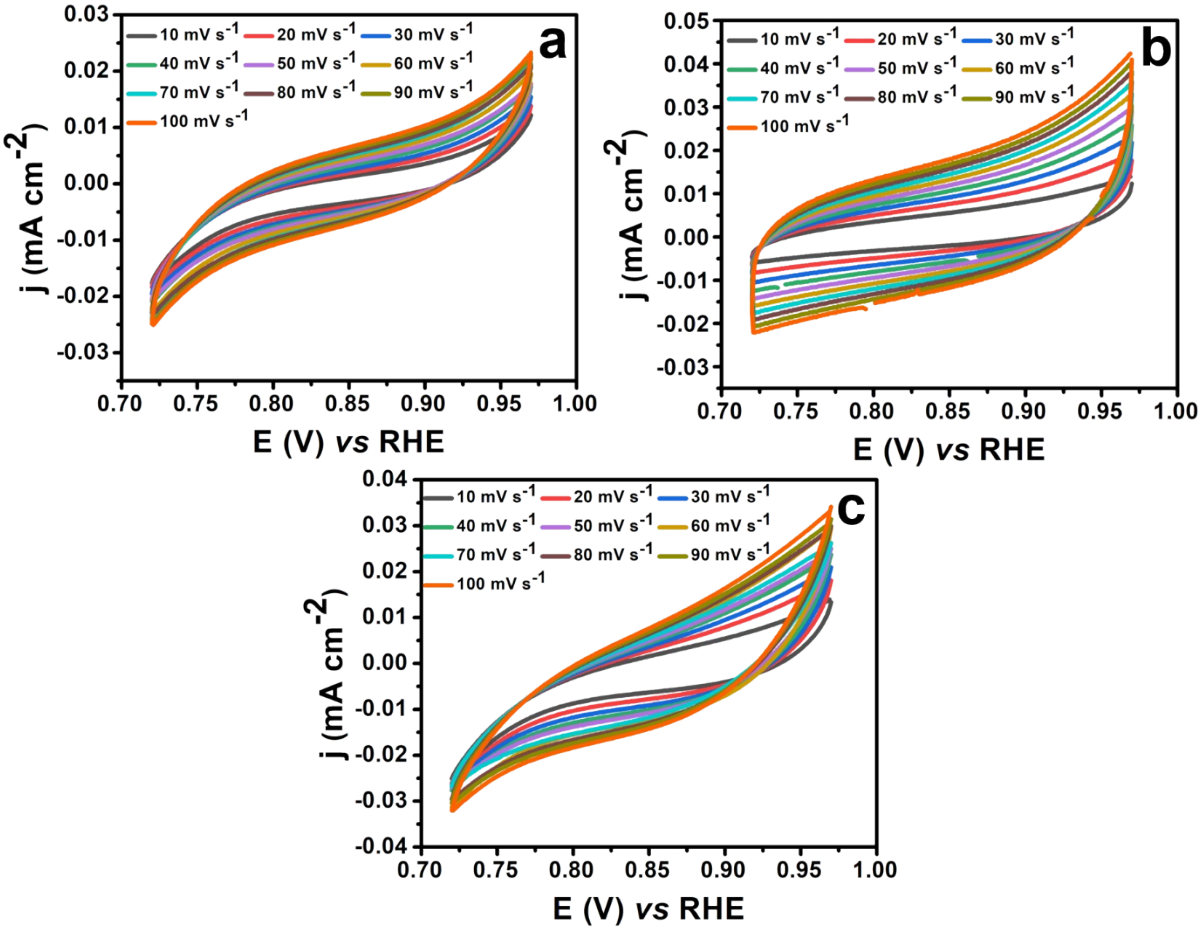

Fig. S7 Cyclic voltammetry curves measured at scan rates from 10-100 mV s^{-1} for (a) Co-Mo control, (b) HNS and (c) HNT respectively.

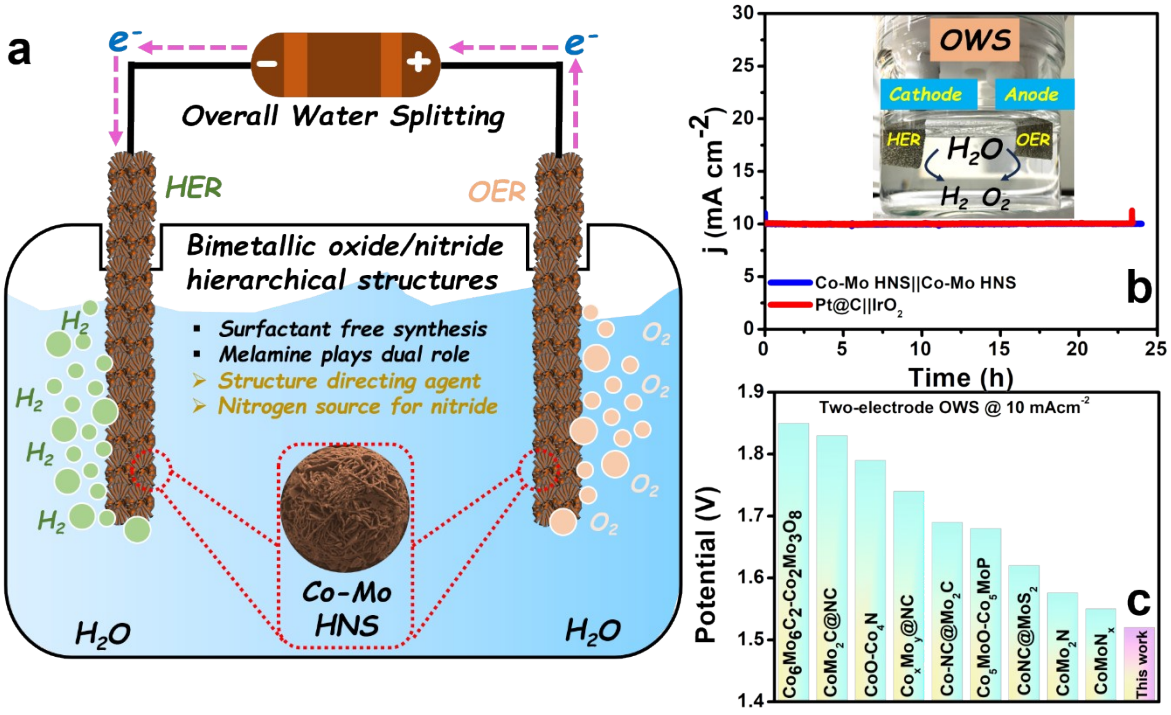

Fig. S8 (a) Illustration of OWS in two-electrode configuration, (b) current density observed over constant cell voltage of 1.52 V for Co-Mo HNS (inset: Experimental setup), and (c) comparison for bifunctional electrocatalyst potentials at 10 mA cm^{-2}.

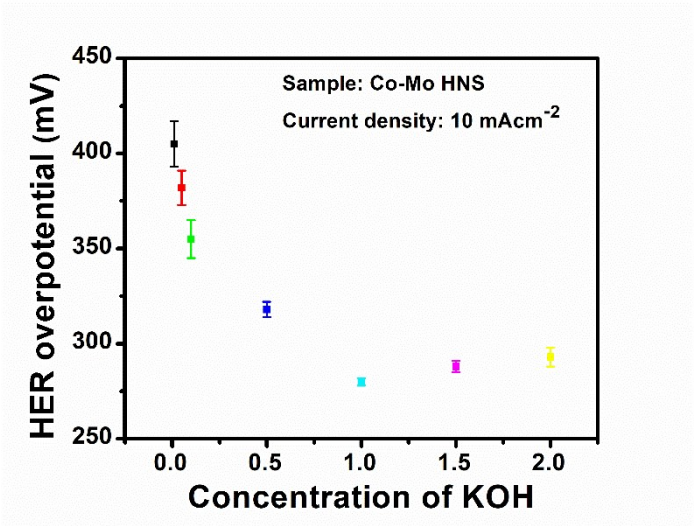

Fig. S9 Concentration of KOH *vs.* HER overpotential responses at the current density of 10 mA cm^{-2}.

Table S4 compares the values of Tafel slopes for HER and OER, capacitive values and cell voltage for different Co-Mo based catalysts measured at 10 mA cm^{-2}.

Electrocatalyst	**Tafel slopes (mV dec^{-1})**		**C_{dl} (µF cm^{-2})**	**Cell voltage (V)**	**Ref.**
	HER	**OER**			
Co_xMo_y@NC	73.5	48.7	7	1.74	[1]
Co-NC@Mo_2C	65	61	85.82	1.69	[2]
Co_5MoO-Co_5MoP	190.1	54.4	-	1.68	[3]
Co-Mo_2N	47	90	42.8	1.58	[4]
CoO-Co_4N	80	83	2.92	1.79	[5]
Co-Mo_2C@NC	118	156	-	1.66	[6]
$Co_3O_4/MoO_3/Mo_xN_y$	119	60.4	20.6	1.52	This work

References

1 J. Jiang, Q. Liu, C. Zeng and L. Ai, *J. Mater. Chem. A*, 2017, **5**, 16929–16935.
2 Q. Liang, H. Jin, Z. Wang, Y. Xiong, S. Yuan, X. Zeng, D. He and S. Mu, *Nano Energy*, 2019, **57**, 746–752.
3 Y. Zhang, Q. Shao, S. Long and X. Huang, *Nano Energy*, 2018, **45**, 448–455.
4 X. Shi, A. Wu, H. Yan, L. Zhang, C. Tian, L. Wang and H. Fu, *Journal of Materials Chemistry A*, 2018, **6**, 20100–20109.
5 R.-Q. Li, P. Hu, M. Miao, Y. Li, X.-F. Jiang, Q. Wu, Z. Meng, Z. Hu, Y. Bando and X.-B. Wang, *Journal of Materials Chemistry A*, 2018, **6**, 24767–24772.
6 M. Wang, S. Dipazir, P. Lu, Y. Wang, M. Yuan, S. Li and G. Zhang, *Journal of Colloid and Interface Science*, 2018, **532**, 774–781.